

Faint dwarfs as a test of DM models: WDM vs. CDM

F.Governato^{1,*}, D.Weisz^{1,2,3}, A.Pontzen⁴, S.Loebman⁵, D.Reed⁶, A. M.Brooks⁷,
P.Behroozi⁸, C.Christensen⁹, P.Madau², L.Mayer¹⁰, S.Shen², M.Walker¹¹,
T.Quinn¹, B.W.Keller¹² and J.Wadsley¹²

¹*Astronomy Department, University of Washington, Box 351580, Seattle, WA, 98195-1580*

²*Dept. of Astronomy, University of California at Santa Cruz, 1156 High Street, Santa Cruz, CA, 95064 USA; drw@ucsc.edu*

³*Hubble Fellow*

⁴*UCL, Department of Physics & Astronomy, Gower Place, London WC1E 6BT, UK*

⁵*Postdoctoral Fellow, Michigan Society of Fellows, Univ. of Michigan, Astronomy Dept., 830 Dennison 500 Church St. Ann Arbor, MI 48109*

⁶*Institut de Ciències de l'Espai (ICE, IEEC-CSIC), 08193 Bellaterra (Barcelona), Spain*

⁷*Dept. of Physics & Astronomy Rutgers Univ. 136 Frelinghuysen Rd, Piscataway, NJ 08854*

⁸*Giacconi Postdoctoral Fellow, Space Telescope Institute, Baltimore, MD*

⁹*Department of Astronomy, University of Arizona, 933 North Cherry Avenue, Rm. N204, Tucson, AZ 85721-0065, USA*

¹⁰*Center for Theoretical Astrophysics and Cosmology, Institute for Computational Science, Zurich, Switzerland*

¹¹*McWilliams Center for Cosmology, Carnegie Mellon University, Pittsburgh, PA 15213*

¹²*Dept. of Physics and Astronomy, McMaster Univ., Hamilton, Ontario, L8S 4M1, CA*

Submitted March 1st, 2014

ABSTRACT

We use high resolution Hydro+N-Body cosmological simulations to compare the assembly and evolution of a small field dwarf (stellar mass $\sim 10^{6-7}M_{\odot}$, total mass $10^{10}M_{\odot}$) in Λ dominated CDM and 2keV WDM cosmologies. We find that star formation (SF) in the WDM model is reduced and delayed by 1-2 Gyr relative to the CDM model, independently of the details of SF and feedback. Independent of the DM model, but proportionally to the SF efficiency, gas outflows lower the central mass density through ‘dynamical heating’, such that all realizations have circular velocities $< 20 \text{ km s}^{-1}$ at 500 pc, in agreement with local kinematic constraints. As a result of dynamical heating, older stars are less centrally concentrated than younger stars, similar to stellar population gradients observed in nearby dwarf galaxies. Introducing an important diagnostic of SF and feedback models, we translate our simulations into artificial color-magnitude diagrams and star formation histories in order to directly compare to available observations. The simulated galaxies formed most of their stars in many ~ 10 Myr long bursts. The CDM galaxy has a global SFH, HI abundance and Fe/H and alpha-elements distribution well matched to current observations of dwarf galaxies. These results highlight the importance of directly including ‘baryon physics’ in simulations when 1) comparing predictions of galaxy formation models with the kinematics and number density of local dwarf galaxies and 2) differentiating between CDM and non-standard models with different DM or power spectra.

Key words: Galaxies: formation – Cosmology – Hydrodynamics, dwarf galaxies, Galaxy Formation.

1 INTRODUCTION

Rapid advancements in numerical and semianalytic techniques and modeling of star formation (SF) and feedback processes have lead to studies of how dark mat-

ter and baryons assemble into cosmic structures within the Λ Cold Dark Matter (CDM) scenario (Robertson et al. 2004; Dutton & van den Bosch 2009; Frenk & White 2012; Benson et al. 2013). At the same time, strong observational evidence has shown how a large fraction of the energy from stellar and quasi-stellar processes couple to the surrounding interstellar medium at all redshifts (McQuinn et al. 2010; van der Wel et al. 2011). SF-related energy coupling

* E-mail:(FG); fabiog@astro.washington.edu

(or ‘feedback’) to the interstellar medium (ISM) is necessary to regulate SF and quench the formation of bulges (Brook et al. 2011; Behroozi et al. 2013a; Hopkins et al. 2013; Munshi et al. 2013).

Recent studies have shown how feedback not only regulates star formation, but directly affects the DM distribution. Rapid (faster than the local dynamical time) removal of gas at sub-kpc scales causes rapid and repeated fluctuations in the gravitational potential, resulting in energy transfer to the dark matter (DM) component, significantly lowering the central density of DM halos (Mashchenko et al. 2008; Governato et al. 2010, 2012; Pontzen & Governato 2012; Martizzi et al. 2013; Di Cintio et al. 2013; Pontzen & Governato 2014). The bursty nature of SF that leads to lower galaxy central densities has strong support from observations (Kauffmann 2014) and when properly incorporated into simulations, results in galaxies with photometric and kinematic properties close to those of real ones (Governato et al. 2009; Oh et al. 2011; Christensen et al. 2014a; Kassin et al. 2014). Combined estimates of the abundance and internal mass distribution of faint field galaxies are now constraining models of galaxy formation in CDM cosmologies, which seem to over predict the number abundance and central density of halos with mass $<10^{10}M_{\odot}$ (Moore et al. 1998; Walker et al. 2010; Papastergis et al. 2011; Garrison-Kimmel et al. 2014a; Kirby et al. 2014; Klypin et al. 2014). Motivated by discrepancies between CDM predictions and observational evidence, theoretical models have also started to explore how ‘non-standard’ models would affect the assembly and inner structure of galaxies. Together with dynamical Dark Energy scenarios (Penzo et al. 2014), recent works have explored physically motivated DM models that specifically alter the number of small DM halos or lower their central DM density, such as warm DM (WDM) and Self Interacting DM (SIDM) (Spergel & Steinhardt 2000; Buckley & Fox 2010; Tulin et al. 2013; Zavala et al. 2013; Vogelsberger et al. 2014),

By damping density perturbations below a streaming length dependent on the particle mass, WDM models reduce the abundance of small halos and delay the collapse of halos above it (Calura et al. 2014). Introducing WDM then lowers the slope of the faint end of the galaxy luminosity function (Menci et al. 2012) and the abundance of Milky Way satellites (Lovell et al. 2012). Analyses of the first simulations explicitly including WDM and gas dynamics have also suggested that galaxy formation in WDM could reduce the mass of stellar bulges (Governato et al. 2004; Herpich et al. 2013), by reducing the number of mergers and interactions. A 2keV WDM scenario can also be used as a maximal case for a class of models advocating for a non-trivial, ‘rolling index’ power spectrum of density perturbations which reduces power at dwarf scales (Garrison-Kimmel et al. 2014b; Hazra et al. 2014), but without the abrupt filtering scale associated with WDM.

Unfortunately, most of the astrophysically driven support for non-standard DM models has come from simulations that neglected the complexities of ‘baryon physics’ and followed only the the assembly of the DM component. This approach has weak predicting power when it comes to comparisons with the observed properties of real galaxies and does not fully take advantage of available con-

Run ID	SF Model	Stellar Mass CDM/WDM	HI mass CDM/WDM
g1	metal cooling, UV	$4.8/1.3 \times 10^6$	$17/36 \times 10^6 M_{\odot}$
g3	g1+HI self-shielding	$8.0/3.0 \times 10^6$	$9.2/14 \times 10^6 M_{\odot}$
g5	g3+Early Feedback	$3.1/0.6 \times 10^6$	$5.0/7.2 \times 10^6 M_{\odot}$

Table 1. *The SF and feedback models used in the simulations vs the $z=0$ stellar and HI masses (in M_{\odot}) for both CDM and WDM cosmologies. $z=0$ stellar masses were measured within 2.5kpc. The WDM realizations have significantly lower stellar masses and higher HI/stellar mass ratios, independently of the SF implementation.*

straints. Specifically, space-based surveys such as the ACS Nearby Galaxy Survey Treasury (or ANGST, Weisz et al. 2011; Ott et al. 2012), that map the spatial distribution and colors of resolved stellar populations allow us to reconstruct the detailed SFHs and metal enrichment histories of the gas and stellar content of nearby dwarf galaxies (Johnson et al. 2013; Weisz et al. 2014). Surveys as the Sloan Digital Sky Survey (SDSS) provide information on the stellar content and instantaneous SF of dwarf galaxies (Kauffmann 2014). Data from these combined observations provide new powerful tests for both SF and dark matter models.

As a CDM model coupled to gas outflows has been shown to lower the central densities of galaxies and quench SF in small systems, ‘baryon physics’ could then remove the need for non-standard DM models, which were introduced to solve the same problems. However, the very low SF efficiency in galaxies forming less than $10^7 M_{\odot}$ in stars may not provide sufficient energy to create DM cores in their host halos Governato et al. (2012); Peñarrubia et al. (2012); Di Cintio et al. (2013). The above arguments strongly suggest that an explicit inclusion of baryon physics in simulations is necessary to investigate the separate effects of SF and feedback from the possible unique signature of a non-standard DM model, high resolution predictions of kinematics and SFHs needs to be extended to the properties of the smallest field dwarfs. In this work we will analyze very high resolution simulations of dwarf galaxies in CDM vs WDM cosmologies, to compare their detailed SFHs together with the evolution of the DM distribution at the centre of their host halos. In §2 and §3 we describe the simulations and the code used, In §4 we discuss the assembly of the baryon and DM components in the two cosmologies. In §5 we discuss the properties of the stellar component, in §6 will describe the mass and DM distribution at their center and summarize the results in §7. We provide additional details on our analysis and artificial observations in Appendix A.

2 THE TREE+SPH CODE CHANGA: A NEW VERSION OF GASOLINE

The simulations discussed in this paper were run in a full cosmological context down to a redshift of zero using the N -body Treecode + Smoothed Particle Hydrodynamics (SPH) code CHANGA (Jetley et al. 2008; Quinn et al. 2013). main novelty consists in the dynamic load balancing and computation/communication overlap provided by the CHARM++ run-time system (Kale & Krishnan 1996). CHANGA scales

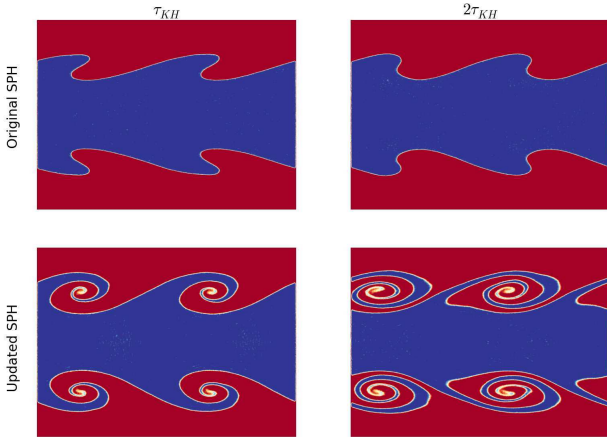


Figure 1. The growth of a Kelvin-Helmholtz (KH) instability at 1 and 2 KH times (τ_{KH}). The top row shows how, using the “traditional” SPH method used in ChaNGa and GASOLINE (Wadsley et al. 2004) spurious surface tension acts to suppress the growth of the KH instability. With the inclusion of a turbulent diffusion term to properly address mixing (Shen et al. 2010) and an alternate force expression (Ritchie & Thomas 2001) this problem is alleviated, and instabilities can grow as they should. This updated SPH method captures mixing in multi-phase gas (an important feature for galaxy simulations) much more accurately.

up to 100,000+ cores and down to only 5,000 particles per core. The communication and multisteping approach, together with extensive scaling tests and a general description of the code are presented in (Menon et al. 2014). CHANGA uses the same hydrodynamic and physics modules previously introduced in GASOLINE (Wadsley et al. 2004; Stinson et al. 2006; Wadsley et al. 2008) together with some improvements to the SPH approach that have already described in the literature (see below). The developers of CHANGA and GASOLINE are part of the AGORA group, a research collaboration with the goal of comparing the implementation of hydrodynamics in cosmological codes (Kim et al. 2014).

Recent works (Agertz et al. 2010) have highlighted how the modeling of pressure gradients in early SPH implementations (Springel 2005) created artificial surface tension between cold dense gas and the hot, more dilute phase. A first step to improve physics at hot-cold interfaces was the addition in CHANGA/GASOLINE of a physically-motivated model for thermal diffusion, described in Shen et al. (2010). We note that all codes, including SPH, have low effective Reynolds numbers compared to real astrophysical flows and thus the required turbulent mixing must often be treated explicitly. We verified that results (and especially the metallicity distribution of stellar populations) do not depend on the details of the mixing model. A key change in CHANGA/GASOLINE is the elimination of artificial gas surface tension through the use of a geometric density mean in the SPH force expression: $(P_i + P_j)/(\rho_i \rho_j)$ in place of $P_i/\rho_i^2 + P_j/\rho_j^2$ where P_i and ρ_i are particle pressures and densities respectively (Ritchie & Thomas 2001). This update better simulates shearing flows with Kelvin-Helmholtz instabilities (Fig 1) and avoids the artificial formation of cold

blobs in smooth flows (Menon et al. 2014). Detailed tests of the updated SPH, as implemented in ChaNGa and Gasoline will be presented in Wadsley et al. (2014 in prep.). Equivalent SPH improvements have been proposed and shown to alleviate artificial surface tension and correctly model strong shocks (Read et al. 2010; Saitoh & Makino 2013; Hopkins 2013). Note that some authors preferentially track entropy rather than energy but all these newer implementations use a geometric density mean for the forces. Further independent testing of these approaches with successful results on a wide range of problems has been presented by Kawata et al. (2013). Thus, there appears to be a growing consensus on the essential ingredients for a modern SPH implementation that can correctly treat the transonic and supersonic flows ubiquitous in astrophysics.

3 CDM AND WDM SIMULATIONS AND STAR FORMATION PARAMETERS

We simulated a single halo in a filamentary region of average density identified in a low resolution, 25 Mpc per side uniform volume simulation that assumed a Λ CDM cosmology ($\Omega_0 = 0.24$, $\Lambda = 0.76$, $\sigma_8 = 0.77$ and $n=0.96$). The halo was then resimulated at high resolution in CDM and WDM cosmologies using the zoom-in technique (Katz & White 1993). The gravitational force spline softening length was set at 60 pc (Power et al. 2003) and a the minimum gas smoothing length (roughly corresponding to the nominal resolution for hydro forces) at 6pc. DM, gas and star particles (when first created) have masses of 6650, 1410, and 422 M_\odot , respectively. With a time evolving mass due to stellar evolution (Wadsley et al. 2004), metallicity of the parent gas particle and fixed IMF, each star particle is effectively a single stellar population. The resolution of these simulations is equivalent to a uniform grid of 4096^3 particles over the entire original volume, and is among the highest published for cosmological simulations carried to $z=0$. By preserving the wave phases in the two simulations, the ‘zoomed in’ approach allows us to isolate the effect of changing the power spectrum on the assembly of individual galaxies and preserving the large scale structure (see also Governato et al. (2004) and Herpich et al. (2013) for a similar approach).

The WDM cosmology adopted here assumes a 2 keV particle and the transfer function was obtained following the fitting formula in Viel et al. (2005). This is the ‘warmest’ model marginally allowed by current constraints (Schneider et al. 2014; Viel et al. 2013); it has been chosen to emphasize the possible differences between CDM and other models with reduced small scales power. The thermal component of the initial velocity field is negligible at the resolved scales. The accuracy of the WDM halo mass function has been tested by comparing with results from Schneider et al. (2012). Due to its lack of power at smaller scales, the WDM simulation starts at $z=119$, while its CDM counterpart starts at $z=129$. Following Lovell et al. (2012), we expect numerical fragmentation effects due finite force and mass resolution (Angulo et al. 2013) to become negligible at halo masses below a few times $10^7 M_\odot$. Empirically, we verified that the typical artificial halos originated by fragmentation have typically 300 DM particles within their virial radius, corresponding to $\sim 2 \times 10^5 M_\odot$. These small halos

DM model	DM/Gas particle mass	Gravtn. Softening	z=0 Halo Mass (DM-only run)
CDM(WDM)	6650/1410	60	$1.16(1.12) \times 10^{10}$

Table 2. *Simulation and Halos Properties.* Column (2) lists the mass (in M_{\odot}) of individual dark matter and star particles in the high resolution region. Column (3) shows ϵ , the spline gravitational force softening (4) lists the halo mass at $z=0$ for the DM-only runs (in M_{\odot}). The minimum smoothing length for the SPH calculation is set to 0.1 the gravitational softening.

contain no gas and oftentimes do not survive the tidal field of larger host halos. We also verified that no stars form in halos with mass below $10^{7.5} M_{\odot}$ at any time in the simulation, providing strong support to the notion that spurious WDM halos do not affect our results.

3.1 Cooling, Star Formation and Feedback

CHANGA tracks the non-equilibrium abundances of H and He. In addition to H and He cooling processes, we include cooling from metal lines, metal diffusion (Shen et al. 2010) and Compton cooling. A uniform, time variable cosmic UV field from Haardt & Madau (2012) models photoionization and heating. We assume that the cosmic UV field is generated in structures above the WDM filtering scale, and it is then identical in the two cosmologies. An approximate treatment of self-shielding is included in some runs following Pontzen et al. (2010): for each gas particle the strength of the UV background used for ionization equilibrium and heating calculations was reduced by the mean attenuation for particles of that density. The SF and blastwave feedback recipes are similar to Governato et al. (2010). Briefly, star formation occurs stochastically when cold ($T < 10^4$ K), virialized gas reaches a threshold density, and follows a Schmidt law:

$$\frac{d\rho_*}{dt} = 0.1 \frac{\rho_{\text{gas}}}{t_{\text{dyn}}} \propto \rho_{\text{gas}}^{1.5}, \quad (1)$$

where ρ_* and ρ_{gas} are the stellar and gas densities and t_{dyn} is the local dynamical time. The force resolution of our simulation enables us to adopt a density threshold for star formation of $100 \text{ atoms cm}^{-3}$, as the local Jeans length at this density and a gas temperature of $T = 10^3$ K is resolved with more than 6 SPH smoothing lengths. A Kroupa (Kroupa 2001) IMF is assumed. For consistency with our previous works that reproduced the properties of galaxies over a range of scales, supernova feedback is implemented according to the blastwave feedback scheme (Stinson et al. 2006), where, in order to prevent artificial cooling of gas particles heated by SNe, cooling is temporarily shut off for typically a few million years. The result of limiting star formation to dense gas regions is that feedback energy is concentrated and, therefore, able to drive outflows (Agertz & Kravtsov 2014). In this work we adopted the same SF parameters (density threshold 100 amu/cm^3 , $c_* = 0.1$ and 100% of SN energy coupled to the ISM) as in Shen et al. (2014). We have verified that this SF approach generates realistic SF efficiencies similar to simulations where the SF efficiency is driven by the local H_2 fraction (Christensen et al. 2014b). The wind loading factors generated by the ‘blastwave’ model

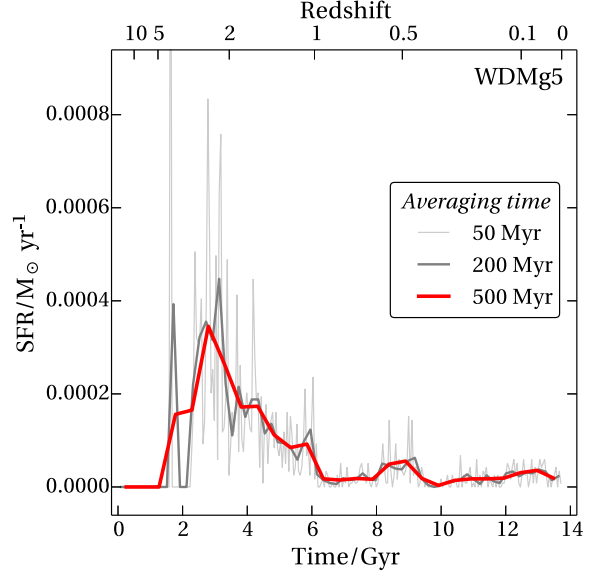


Figure 3. *The SFR of the galaxy in the WDM cosmology.* SFR is measured including all the stars within the central 1kpc $t = z=0$. The reference WDMg5 run has delayed SF compared to the CDM runs. The WDM run forms less stars overall. This delay is independent of the details of SF and feedback.

are slightly lower than in a scheme where the time scale for inefficient cooling is explicitly regulated by a conduction subgrid model (Keller et al. 2014) which we plan to adopt in future works.

Each CDM and WDM halo was run several times, following a sequence of increasing complexity in the description of ISM physics and SN feedback that was identical for both cosmologies. This sequence of runs has the specific goal of differentiating the effects of changing the DM ‘scaffolding’ vs the effects of using different implementations of SF-related processes (see Table 1). Runs ‘g1’ include metal cooling, cosmic UV and SN feedback, ‘g3’ include also HI shielding from UV radiation, while ‘g5’ also include ‘early’ feedback from young stars following Stinson et al. (2012). The amount of energy from young stars (often referred to as ‘early feedback’ that is injected into the ISM as thermal feedback is 10^{49} erg per solar mass of stars formed. Cooling of the gas is not shut-off for ‘early feedback’. The total amount of energy injected into the ISM is then $\sim 2 \times 10^{49} / M_{\odot}$ of stars formed, comparable to the energy coupled to the ISM in other recent stellar feedback schemes (Hopkins et al. 2013; Vogelsberger et al. 2013; Anglés-Alcázar et al. 2014). *This work focuses on the ‘g5’ runs*, as they include the most complete description of ISM and feedback physics. For reference, the SF and feedback of the ‘g5’ model resembles the one in Di Cintio et al. (2014), while ‘g1’ resembles the runs in (Shen et al. 2014). However, those previous runs do not include the new SPH implementation. We highlight the differences between the different implementations at different points in the paper. We plan to extend our analysis to a large sample of small systems in future work.

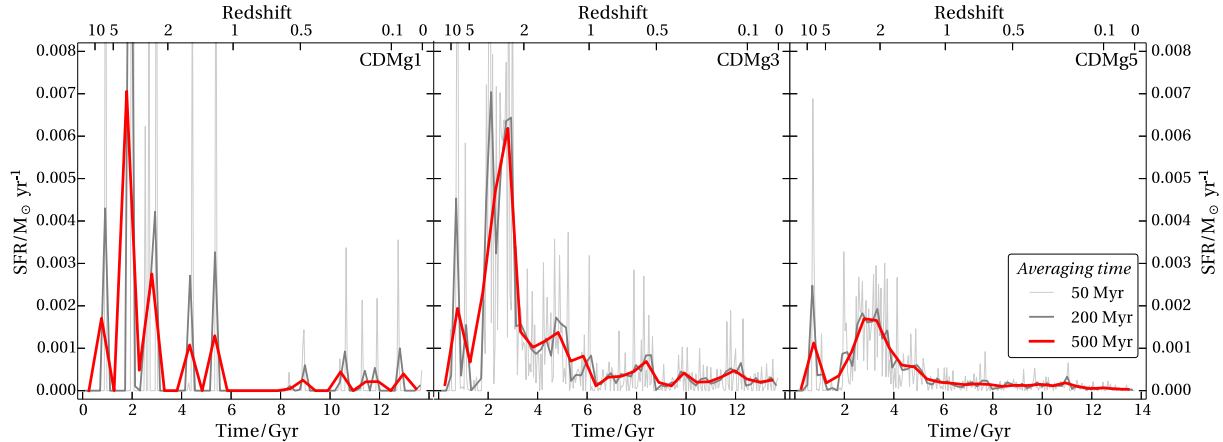


Figure 2. The SFR of the galaxy in the CDM cosmologies with different time binsize. SFR is measured including all the stars within the central 1kpc at $z=0$. The lack of self-shielding in CDMg1 gives sparse and very bursty SF. The SFH histories of the g3 (which includes self-shielding) and g5 (self-shielding and ‘early’ feedback) runs, are composed of many, short (~ 10 Myrs) bursty events. During these bursts, SF increases by a factor ranging from 1 to 10 compared to the local time average. This behaviour is typical in the SFHs of dwarf galaxies obtained from SDSS (Kauffmann 2014). The SFH of runs g3 and g5 become smoother if averaged over longer time intervals that approach what is possible in the deepest observations of LG dwarf galaxies. In all runs the SF events create outflows that lower the central DM density of the host halo (Fig. 7 & Fig. 8).

4 THE ASSEMBLY OF DM AND STARS IN GALAXIES

The main properties of the simulated halo are summarized in Tables 1 & 2. Halos were identified with the halo finder AMIGA (Knollmann & Knebe 2009). By $z=0$, the final halo mass is approximately the same in CDM and WDM cosmologies, as the halo mass ($10^{10} M_{\odot}$) is above the 2keV filtering scale. The main halo accumulated 50% of its final mass by $z \sim 2.5$ in both cosmologies. However, the assembly histories are markedly different at higher z where the filtering of small scales in the WDM model becomes important. At $z=4$, 25% of the CDM halo final mass is in collapsed, star forming progenitor haloes, while the main progenitor of the WDM halo contains only 7% of its final mass. This delay in halo assembly is typical of WDM cosmologies implying that SF is absent or minimal during the first two Gyrs (compare Fig. 2 with Fig. 3). A delayed SF in WDM models, especially in small systems, had been recently suggested in a semi analytical model (Calura et al. 2014). Most of the baryons of the WDM galaxy accreted onto the main halo from smooth accretion and not through mergers with smaller halos. The SFH of models including shielding (g3 and g5) and early feedback from young stars (g5) are extended, with several small bursts occurring over the whole Hubble time. the ‘CDMg1’, which lacks both the above physical processes shows a more intermittent, very bursty SF.

By $z=0$, ‘g5’ galaxies in both cosmologies show a rotationally flattened stellar component and an extended HI disc, with no sign of a central bulge component. However the stellar disk is quite thick and dynamically hot. Thick stellar disks are a characteristic of feedback implementations that model radiation or stellar winds from young stars (Stinson et al. 2013; Trujillo-Gomez et al. 2013; Hopkins et al. 2013). By $z=0$, the amount of stars formed in the WDM model is only 20-40% of the CDM counterpart, depending on the specific SF model adopted: ‘g3’ runs (where gas is shielded) form the largest amount of stars,

while ‘g5’ (where feedback from young stars is also included) form the least. While all CDM realizations show a cold gas/stars mass ratio around one or larger when measured at $z=0$, WDM models are several times more HI rich than observed dwarfs of similar mass, which typically have HI/stellar mass ratios closer to unity (Geha et al. 2006; McConnachie 2012). We speculate that the longer depletion time scale of cold gas in WDM could be due to a drastically reduced interaction rate with dark subhalos, which could induce disk instabilities (Chakrabarti 2013; Herpich et al. 2013). Alternatively, this could also be due to the later assembly of the WDM halo and the delayed onset of gas cooling, which then settles in a larger, lower density disk. We verified that the WDM halo accretes only one subhalo with circular velocity $V_c > 10$ km/sec, at $z \sim 3^1$.

5 SFH HISTORIES AND COLOR MAGNITUDE DIAGRAMS

In this work we compare the SFHs of our models with those of the galaxies in two HST studies: the ANGST sample and of a subsample of field Local Group dwarfs with deeper observations than ANGST (Weisz et al. 2014). The SFHs of the real galaxies were reconstructed from the analysis of their resolved stellar populations (Dolphin 2002; Tolstoy et al. 2009; McQuinn et al. 2010). For the purpose of comparing simulations with observations is important to note that the typical region of each galaxy surveyed by HST varies with the galaxy distance. Galaxies in the ‘Local Group’ sample have been observed to fainter magnitudes, but only out to (typically) 100-300 pc. Stellar populations in the ANGST sample have been typically observed out to 1-2kpc from the dwarf centre. This aperture effect may lead to potential biases in the reconstruction of their SFHs. We

¹ V_c is defined as $\sqrt{M/r}$ throughout the paper, with $G=1$

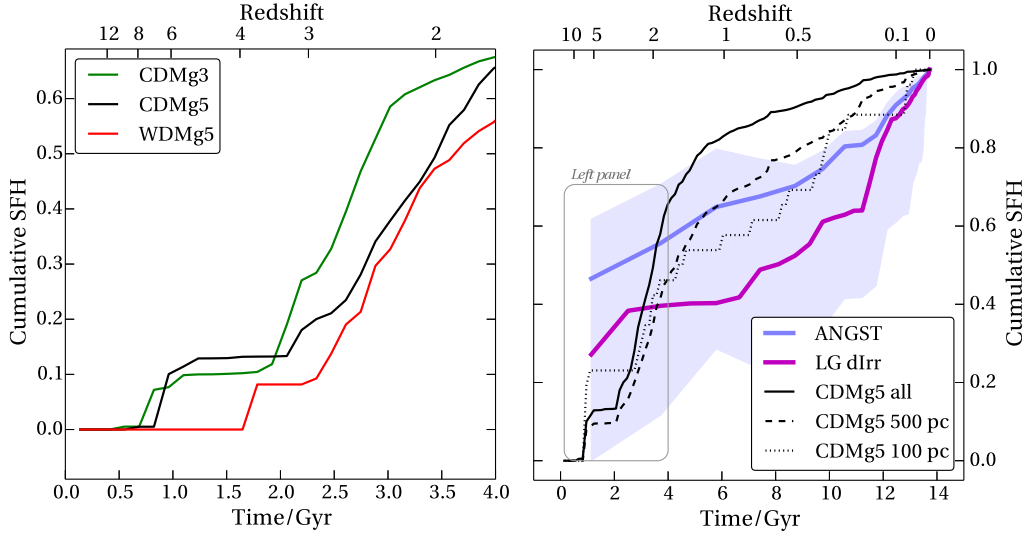


Figure 4. *Left:* The cumulative SFH (i.e., the fraction of total stellar mass formed prior to a given epoch, normalized to one at the present) within the 500 pc of the simulated galaxy in the CDM and WDM cosmologies. CDM: solid (g5), green (g3) lines, WDM (g5): red line. Overall the SFH of the simulated galaxy reproduces the rapid rise and the subsequent linear growth of the ANGST sample (see right panel), but SF starts one Gyr later in the WDM model. *Right:* The cumulative SFH as a function of aperture of our standard implementation CDMg5. The SFH from the simulation is measured including spherical regions of different radius, but all centered on the galaxy center (black: all, dashed: 500 pc, dotted: 100 pc). ANGST average: blue, Local group: magenta. The shaded area shows the dispersion of the ANGST sample. The differences in the simulated SFHs illustrate how the center of the simulated galaxy is populated by younger stars while the outer regions consists mainly of older stars, likely scattered outward during the process of core formation. This radius vs age bias may explain the difference between the ANGST and the LG sample, the latter sample stars in the very central regions (55-300 pc) of relatively nearby systems.

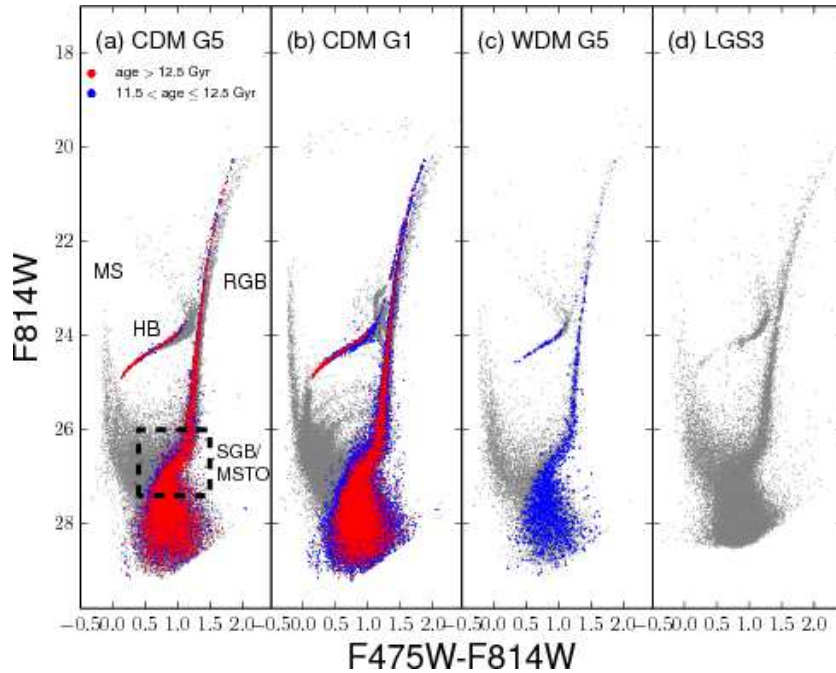


Figure 5. Mock color-magnitude diagrams (CMDs) for select galaxies from our simulations. The CMDs have been designed to mimic deep HST observations of Local Group dwarf galaxies (Cole et al. 2007). We have highlighted features important for measuring the SFH of a galaxy (upper main sequence, MS; red giant branch, RGB; horizontal branch, HB; sub-giant branch, SGB; oldest main sequence turn-off, MSTO and color-coded stars that are between 11.5 and 12.5 Gyr old (blue) and older than 12.5 Gyr (red). CDMg5 (and CDMg3, not shown) has a CMD that is qualitatively similar to those observed in real local dwarfs such as LGS3 (Hidalgo et al. 2011), which is shown in panel (d). In contrast WDMg5 is deficient in ancient stars, as it can be seen by the lack of a blue horizontal branch compared to the LGS3 CMD (at a color of ~ 0.5 and a magnitude of ~ 24.7). CDMg1 (the run with no self-shielding and early feedback) contains fewer, discrete bursts throughout its lifetime, neither of which are usually observed in low mass galaxy SFHs.

discuss effects of this aperture bias, and will explore it in the context of simulated population gradients in future work (M.Teyssier et al. in prep.).

Fig. 2 and Fig. 3 show the SFR of the CDM and WDM halos as directly measured in the simulations at $z=0$. The SFHs include only stars less than 1 kpc from the centre of the galaxy, to be consistent with the typical aperture of galaxies in the ANGST sample. Half of the mass in stars is located within a 1 kpc radius from the center in the CDM galaxy, within 700pc in the smaller mass WDM galaxy. In CDM the first stars are formed as early as $z=8$, while in WDM, star formation started one Gyr later, by $z\sim 4$. The 'g1' galaxies (lacking self-shielding) have episodic star formation, while all other runs have bursty, but continuous SF. The 'g3' runs, that include shielding, form about twice as many stars as our standard run 'g5', that includes both self shielding and 'early feedback' from young stars (Table 2). Observations strongly support bursty SFHs in small galaxies, with as many as 80% stars being formed in bursts (Kauffmann 2014) and a relatively high SF efficiency at high z (Madau et al. 2014b).

Fig. 4 shows the cumulative SFHs of the CDM and WDM models against those from the ANGST and Local group samples (Weisz et al. 2014). The average SFH of the ANGST and Local Group samples shows even older populations than our simulated galaxy. This difference likely depends on the detailed assembly history of our galaxy. However, in all our simulations the CDM galaxy forms about 10% of their stellar mass before the WDM galaxy even starts forming stars. This earlier relative start of SF in the CDM models is independent of the SF model used, and persists even when 'early' feedback is included (which overall delays SF, Stinson et al. (2013)). As soon as the WDM galaxy starts forming stars it catches up rapidly and by $z \sim 1.5$, 50% of present day stars have formed in both models. SF after $z = 2$ then depends mostly on the implementation of SF and feedback. Fig 4 (right panel) compares the cumulative SFH of our simulated galaxy CDMg5 compared to the average SFHs of the ANGST Local Group (LG) samples. Analysis of the simulations allows us to understand the difference in the SFHs between the two samples, with the 'LG sample' galaxies apparently having much younger stellar populations. Part of the observed difference can be reproduced by calculating the cumulative SFH of stars selected inside smaller and smaller radii of the simulated galaxy. In CDMg5, only 10% of halo stars (a subsample with minimum distance 1 kpc from the galaxy center) are younger than 8 Gyrs, compared to 40% of the stars within a radius of 200 pc. We verified that at $z=3.4$, the mean radius of all stars in the main halo of CDMg5 is $\langle r \rangle = 0.66$ kpc, while taking those exact same stars but tracing them forward to $z=0$, the mean radius is now $\langle r \rangle = 1.22$ kpc. This finding shows how the same 'dynamical heating' process that removes DM from the galaxy centers can also act on stars (an equally collisionless component), resulting in older stars being moved outward on less bound orbits (see also Maxwell et al. 2012). *Together these results predict real dwarfs to have 1) a significant population of old stars, 2) age gradients, with younger stars being more centrally concentrated. These result are independent of the DM and SF models used in this work.*

In Fig. 5 we show the artificial CMDs obtained from the stellar populations of different simulations in our sample (see Appendix for details). These CMDs include typical observa-

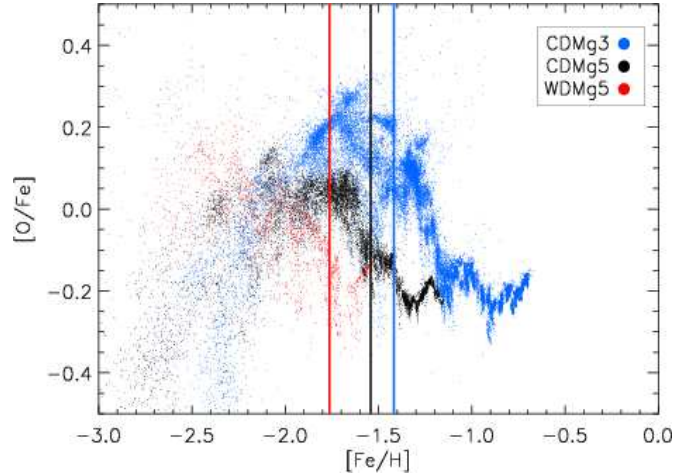


Figure 6. The $[O/Fe]$ vs $[Fe/H]$ for CDMg3, CDMg5 and WDMg5. The abundance trend is set by the SFH rather than the DM model. As 'g3' is the most efficient star former, the ISM is enriched by of SNII (high O/Fe) before the SNIa kick in, and overall it reaches the highest $[Fe/H]$. The g5 runs form less stars, and the initially lower SFR lead to lower O/Fe at low metallicities. The "knee" kicks in at lower $[Fe/H]$ for lower SFR, and the overall highest $[Fe/H]$ reached is just dependent on the total stellar mass formed. The vertical lines show the average metallicity for dwarf galaxies with stellar masses equal to the simulated ones, from Kirby et al. (2014).

tional effects such as resolution and limiting magnitude of HST observations of Leo A, a typical nearby dwarf ~ 800 kpc away: with a CMD completeness limit of ~ 29.0 in F475W and 27.8 in F814W (Cole et al. 2007). These CMDs qualitatively show the features in the SFH described above. The lack of old stars in the WDMg5 run and the very episodic SFH of CDMg1 (the CDM run with no self-shielding) can be clearly identified and are not features commonly observed in the CMDs of nearby dwarf galaxies. Artificial CMDs such as these will be used in future comparisons between observational and simulated samples.

In Fig. 6 we examine metallicity trends in the CDMg3, CDMg5, and WDMg5. We track oxygen as a proxy for α abundances. Overall, the chemical trends are driven by the SFH of each simulation. CDMg3 is the simulation with the most efficient star formation. With a higher early SFR then the g5 models (twice as many stars formed in the first 3 Gyrs), CDMg3 is initially dominated by enrichment from SNII, with a high $[O/Fe]$ ratio. At later times, SNIa begin to contribute predominantly Fe, causing the $[O/Fe]$ to drop as $[Fe/H]$ increases. Because it forms the most stars overall, CDMg3 reaches the highest $[Fe/H]$ of any of the models. The g5 runs, on the other hand, have such low SFRs that SNIa are able to contribute at lower $[Fe/H]$. The 'knee' in these plots occurs at lower $[Fe/H]$ for a lower SFR, and the runs that form the most stars are able to reach a higher $[Fe/H]$ ultimately. The vertical lines show the mean $[Fe/H]$ of field dwarfs of similar stellar mass as their color coding from Kirby et al. (2014). While a direct comparison would require a more detailed comparison (M.Teyssier et al. in prep.) they show that the average metal content of the simulated galaxies is consistent with observations.

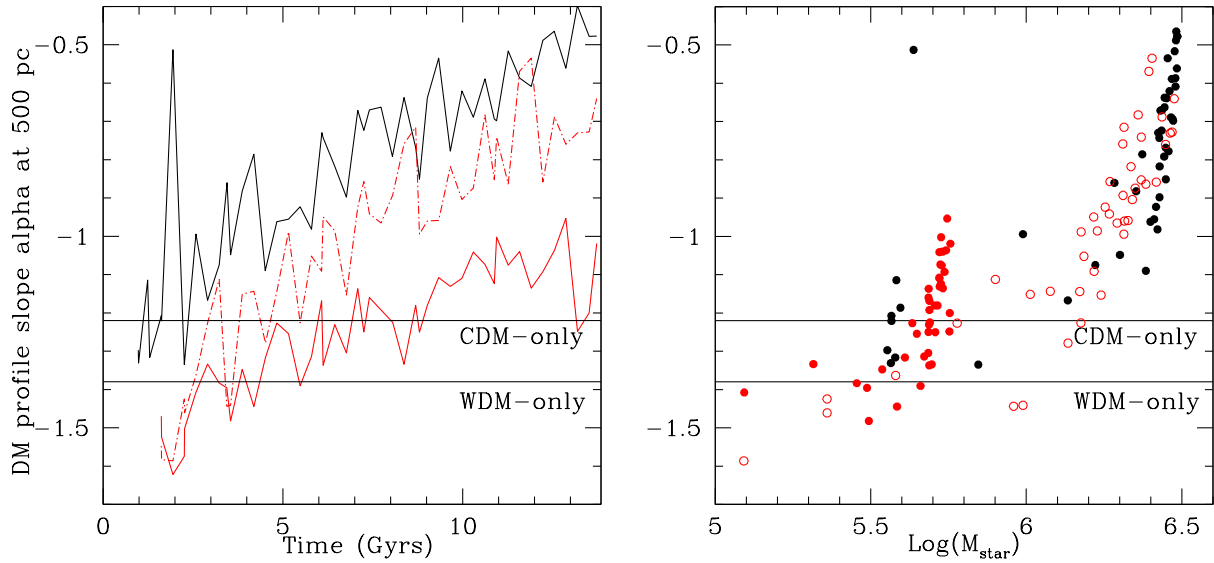


Figure 7. *Left:* The time evolution of the slope α of the CDMg5 (solid black) and WDMg5 (solid red) halos, measured at 500 pc. The red dash-dotted line shows the WDMg3 run, which has a higher SF efficiency, leading to a final flatter DM profile. These results highlight how DM ‘heating’ is a continuous process which begins at high- z and depends strongly on the SF efficiency, (higher efficiency leading to flatter profiles) rather than on the details of the CDM vs WDM cosmologies. As a reference, the DM α slopes at $z=0$ of the DM-only simulations are shown as horizontal lines. *Right:* The slope of the DM profile measured at 500 pc vs. the galaxy stellar mass for several time outputs of the main progenitor of CDMg5: solid dots, WDMg5 (solid red) and WDMg3 (red circles). Dashed horizontal lines show the $z=0$ of the equivalent DM-only runs.

6 MASS DISTRIBUTION: EVOLUTION AND COMPARISON WITH OBSERVATIONS

Fig. 7 (left panel) shows the evolution of α (here α is the DM density profile slope measured at 500 pc), for the main progenitor of various models as function of time. This plot emphasizes how the formation of cores is a continuous process driven by prolonged and bursty SF. Core formation happens later in models where halo collapse (as in WDM), or ‘young stars’ feedback, delays the main onset of SF. In Fig. 7. (right panel) we show instead the dependence of α on the amount of stars formed in a few runs. Data points belong to the different progenitors of a given $z=0$ galaxy, so this is equivalent to a time sequence (see also Madau et al. 2014a). The horizontal lines mark the slope of the DM profile in the DM-only runs. This plot shows how the ‘DM heating’ process is important even when only $10^6 M_{\odot}$ of stars have formed, independent of the details of SF and feedback implementations, as long as they create rapid outflows. This results largely confirm those of previous works (Teyssier et al. 2013; Pontzen & Governato 2012; Madau et al. 2014a) in more massive halos. In all simulations cores, once formed, persisted to the present time.

In Fig. 8 we compare the total mass distribution (DM and baryons) of our simulated CDM and WDM dwarf with the observational constraints of a subsample of Local Group field galaxies (from Wolf et al. 2010; McConnachie 2012; Weisz et al. 2014).

The main result is that DM heating lowers the central total matter distribution of field dwarf galaxies, in both CDM and WDM cosmologies. By the present time the central mass distribution of all the runs with SF is remarkably

similar in both cosmologies, with circular velocities at 0.5 kpc of the order of $V_c = \sqrt{M/r} \sim 10$ km/sec, consistent with estimates of local field dwarfs of similar stellar mass. As DM-only simulations often show an excess of central mass in systems with low internal velocities, the introduction of feedback would help bring theoretical predictions in agreement with current kinematic constraints, independently of DM being ‘Warm’ or ‘Cold’. A larger set of galaxies is however required to make more quantitative statements.

Overall these different results show that the mass distribution of dark matter and stars depend more on the efficiency of star formation rather than on the type of DM (CDM vs WDM) or the slope of the primordial power spectrum of density perturbation at small scales. Models with more efficient SF create more DM and stellar ‘heating’, erasing difference driven by the details of initial power spectrum, assembly history and formation times of the parent halos, which affect the DM halo concentration (Garrison-Kimmel et al. 2014a). In following work we will study the number density and observed circular velocities of a large sample of simulated field dwarfs (Brooks & Pappastergis in prep.) and compare the DM profiles of CDM and SIDM halos (Bastidas-Fry et al 2014, in prep.).

7 CONCLUSIONS

We have simulated to $z=0$ the evolution of a small (halo mass $\sim 10^{10} M_{\odot}$) field dwarf galaxy in Λ CDM and Λ WDM cosmologies. Our goal was to identify differences in the observable properties of the galaxy and its DM distribution once baryon processes are included together with non-standard

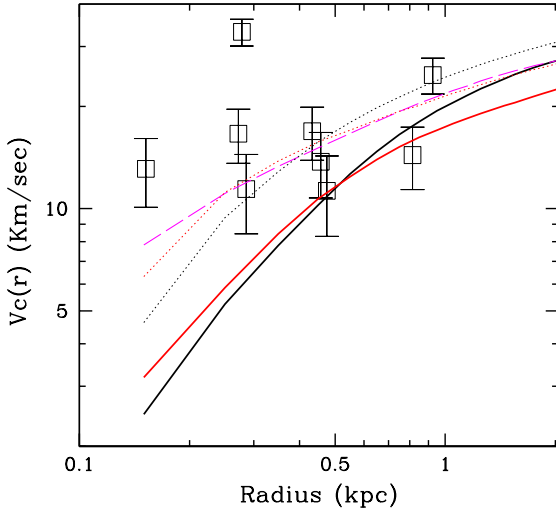


Figure 8. The rotation curve (defined as $V_c = \sqrt{M/R}$, with $G=1$, including both DM and baryonic matter) of the simulated galaxies vs. the observational estimates of field LG dwarfs with stellar masses in the 10^6 - $10^7 M_\odot$ range. Black: CDMg5, Red: WDMg5. Magenta dashed: CDMg1. Black and red dotted: CDM-only and WDM-only runs. Estimates from real galaxies are based on stellar kinematics. Error bars show a representative 5km/sec uncertainty rather than published errors. DM and stellar dynamical ‘heating’ due SF and feedback processes reduce the overall central density, irrespective of the DM component. As a result the amount of mass within the central 500pc (a scale well resolved in these simulations) is lowered. This process will help reconcile prediction of the mass distribution in dwarfs with the current observational constraints from Local Group galaxies

(Wolf et al. 2010; Weisz et al. 2014; Brook & Di Cintio 2014).

DM. These simulations have a nominal force resolution of 60pc and gas forces resolved down to ~ 10 pc. For both cosmologies, we performed a series of runs where we modeled the effects on SF of cold gas shielding and the deposition of energy from young stars in the ISM. The SPH implementation better follows Kelvin-Helmoltz instabilities and gas interactions at the cold/hot interface.

- Due to the later assembly and suppression of substructure in the the WDM model, the WDM and CDM galaxies differ significantly in some properties of their stellar components. In the WDM model, SF begins 1.5 Gyrs later, is more inefficient and results in a galaxy that has a higher and somewhat unrealistic HI/stellar mass ratio (closer to unity in real galaxies and in the CDM realizations). These differences are independent of the details of SF and feedback. The effect of less efficient SF and increased HI mass in WDM models may have a strong effect on the luminosity and velocity distribution function of field galaxies and needs to be studied in larger simulated samples.

- The inclusion of explicit ‘baryonic physics’ is the major driver of the central distribution of galaxies. Rather than being set by intrinsic differences between the Cold and Warm DM models, the matter distribution at the center of field dwarfs is largely set by the amount of stars formed (with more stars forming resulting in the ‘heating’ of larger amounts of DM and stars Maxwell et al. 2012; Di Cintio et al. 2013). By the present time, both CDM and

WDM galaxies show a reduced central density and flatter DM profile compared to their DM-only realizations, making the simulated galaxies consistent with the constraints set by kinematic estimates of the mass content of field dwarfs of similar stellar mass. At this high resolution, DM removal within the central 500 pc becomes significant even as few as $10^6 M_\odot$ stars formed.

- Feedback lowers the central mass content of $10^{10} M_\odot$ halos, bringing them into agreement with observations even when SF is relatively inefficient when compared to standard Abundance Matching models ($M_{star}/M_{halo} \sim 10^{-4}$, see Munshi et al. 2013; Behroozi et al. 2013b). This result shows that the complexity of baryonic processes needs to be explicitly included in models of galaxy formation when comparing the prediction of CDM or other models with the combined constraints from the kinematic and number density of local field dwarfs (Klypin et al. 2014; Brooks & Zolotov 2014).

- A qualitative comparison between artificial CMDs and those obtained with HST on samples of local galaxies favors dwarf galaxies formed in a CDM cosmology, with very old stellar populations and a continuous SF comprised of several small bursts when properly time resolved. When plotted with a low time resolution, the SFH of dwarf galaxies appears smoother, being the superposition of timely and spatially independent SF events. In all galaxies, the older stellar populations are less radially concentrated, possibly the effect of energy transfer not just to the DM but also to stars, going a long way resolving the apparent discrepancy between the average SFH recovered from the full ANGST sample (with typical apertures of 1 kpc) and those of the closest field dwarfs in our Local Group (where the limited HST field covered a much smaller central area, typically of 50-150pc in radius).

This is one of the first works to compare the *observable* properties of the resolved stellar populations of faint field dwarfs with the predictions of CDM and non-standard DM models. Given the sample of just one halo the results are necessarily preliminary. In future work we plan to extend this study to a larger sample, allowing us to predict the number density of field dwarfs Klypin et al. (2014). At high redshift, a DM scenario with reduced small scales power (see also Garrison-Kimmel et al. 2014b) may leave a clear signature in the abundance and SF rates of faint galaxies (stellar mass $10^{7-9} M_\odot$ Atek et al. 2014). In higher redshift systems, the delay in SF in WDM models would be evident in the SFR/stellar mass relation (e.g. Noeske et al. 2007; Puech et al. 2014; Calura et al. 2014). These measurements are now becoming feasible through deep observations of field magnified by lensing clusters (Menci et al. 2012; Pacucci et al. 2013; Alavi et al. 2014; Pandolfi et al. 2014). Future hydrodynamical simulations will help disentangle the effects of SN feedback from that of the underlying DM or dark energy models, provide a robust counterpart to the stronger constraints coming from studies of the properties of small field galaxies, and better guide predictions for DM direct detection experiments (see review by Brooks 2014).

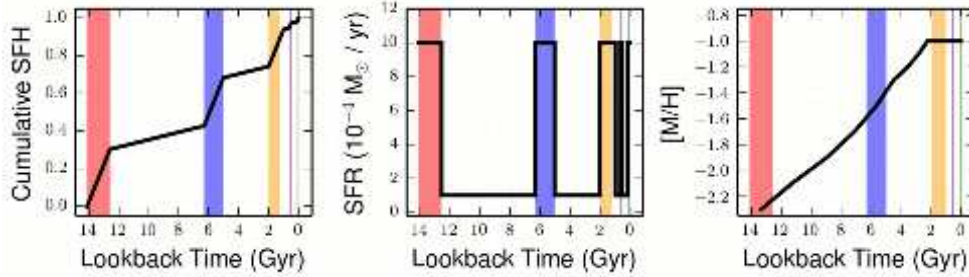


Figure 9. *Appendix A: The mock star formation history (SFH) and age-metallicity relationship (AMR) used to construct the schematic CMDs in Fig. 10* The left panel shows the cumulative SFH, i.e., the fraction of stellar mass formed prior to a given epoch; the center panel shows the absolute SFH; and the right panel shows the AMR. In this model 80% of the stars is formed in bursts. Note that the x-axis shows 'lookback time' and not the time since the Big Bang as in previous plots. In each panel, we have highlighted each burst in color: 0-0.1 Gyr (green), 0.5-0.6 Gyr (purple), 1-2 Gyr (orange), 7-8 Gyr (blue), 12.5-14 Gyr (red). The SFH is modeled after a bursty dwarf galaxy with quasi-periodic bursts superimposed on a low-level constant SFR.

ACKNOWLEDGMENTS

FG and TQ were funded by NSF grant AST-0908499. FG acknowledges support from NSF grant AST-0607819 and NASA ATP NNX08AG84G. Support for DRW is provided by NASA through Hubble Fellowship grants HST-HF-51331.01, awarded by the Space Telescope Science Institute. Simulations were run on Pleiades (NASA HEC) and Blue Waters (XSEDE) supercomputers. ChaNGa was developed with support from National Science Foundation ITR grant PHY-0205413 to the University of Washington, and NSF ITR grant NSF-0205611 to the University of Illinois. Some images were created with the analysis and graphic package Pynbody (Pontzen et al. 2013). SRL acknowledges support from the Michigan Society of Fellows.

REFERENCES

- Agertz O., Kravtsov A. V., 2014, ArXiv e-prints
 Agertz O., Teyssier R., Moore B., 2010, MNRAS, 1527
 Alavi A. et al., 2014, ApJ, 780, 143
 Anglés-Alcázar D., Davé R., Özel F., Oppenheimer B. D., 2014, ApJ, 782, 84
 Angulo R. E., Hahn O., Abel T., 2013, MNRAS, 434, 3337
 Atek H. et al., 2014, ApJ, 789, 96
 Behroozi P. S., Wechsler R. H., Conroy C., 2013a, ApJ, 770, 57
 Behroozi P. S., Wechsler R. H., Wu H.-Y., Busha M. T., Klypin A. A., Primack J. R., 2013b, ApJ, 763, 18
 Benson A. J. et al., 2013, MNRAS, 428, 1774
 Brook C. B., Di Cintio A., 2014, ArXiv e-prints
 Brook C. B. et al., 2011, MNRAS, 415, 1051
 Brooks A. M., 2014, AdPhysik 10.1002/andp.201400068, 10
 Brooks A. M., Zolotov A., 2014, ApJ, 786, 87
 Buckley M. R., Fox P. J., 2010, Physics Review D, 81, 083522
 Calura F., Menci N., Gallazzi A., 2014, MNRAS, 440, 2066
 Chakrabarti S., 2013, ApJ, 771, 98
 Christensen C. R., Brooks A. M., Fisher D. B., Governato F., McCleary J., Quinn T. R., Shen S., Wadsley J., 2014a, MNRAS, 440, L51
 Christensen C. R., Governato F., Quinn T., Brooks A. M., Shen S., McCleary J., Fisher D. B., Wadsley J., 2014b, MNRAS, 440, 2843
 Cole A. A. et al., 2007, ApJL, 659, L17
 Dalcanton J. J. et al., 2009, ApJS, 183, 67
 Di Cintio A., Brook C. B., Maccio A. V., Stinson G. S., Knebe A., Dutton A. A., Wadsley J., 2013, ArXiv e-prints
 Di Cintio A., Brook C. B., Maccio A. V., Stinson G. S., Knebe A., Dutton A. A., Wadsley J., 2014, MNRAS, 437, 415
 Dohm-Palmer R. C. et al., 1997, AJ, 114, 2514
 Dolphin A. E., 2002, MNRAS, 332, 91
 Dutton A. A., van den Bosch F. C., 2009, MNRAS, 396, 141
 Frenk C. S., White S. D. M., 2012, Annalen der Physik, 524, 507
 Gallart C., Monelli M., Dolphin A., Bernard E., Drozdovsky I., Aparicio A., Cassisi S., 2007, in Astronomical Society of the Pacific Conference Series, Vol. 374, From Stars to Galaxies: Building the Pieces to Build Up the Universe, Vallenari A., Tantaló R., Portinari L., Moretti A., eds., p. 253
 Garrison-Kimmel S., Boylan-Kolchin M., Bullock J. S., Kirby E. N., 2014a, ArXiv e-prints
 Garrison-Kimmel S., Horiuchi S., Abazajian K. N., Bullock J. S., Kaplinghat M., 2014b, ArXiv e-prints
 Geha M., Blanton M. R., Masjedi M., West A. A., 2006, ApJ, 653, 240
 Girardi L. et al., 2010, ApJ, 724, 1030
 Governato F. et al., 2010, Nature, 463, 203
 Governato F. et al., 2009, MNRAS, 398, 312
 Governato F. et al., 2004, ApJ, 607, 688
 Governato F. et al., 2012, MNRAS, 422, 1231
 Haardt F., Madau P., 2012, ApJ, 746, 125
 Hazra D. K., Shafieloo A., Smoot G. F., Starobinsky A. A., 2014, ArXiv e-prints
 Herpich J., Stinson G. S., Maccio A. V., Brook C., Wadsley J., Couchman H. M. P., Quinn T., 2013, ArXiv e-prints
 Hidalgo S., Aparicio A., Gallart C., Monelli M., Stetson P. B., Walker A. R., 2010, NOAO Proposal, 194
 Hidalgo S. L. et al., 2011, ApJ, 730, 14
 Hopkins P. F., 2013, MNRAS, 428, 2840
 Hopkins P. F., Keres D., Onorbe J., Faucher-Giguere C.-A., Quataert E., Murray N., Bullock J. S., 2013, ArXiv

- e-prints
- Jetley P., Gioachin F., Mendes C., Kale L. V., Quinn T. R., 2008, in Proceedings of IEEE International Parallel and Distributed Processing Symposium 2008
- Johnson B. D. et al., 2013, *ApJ*, 772, 8
- Kale L. V., Krishnan S., 1996, in Parallel Programming using C++, Wilson G. V., Lu P., eds., MIT Press, pp. 175–213
- Kassin S. A., Brooks A., Governato F., Weiner B. J., Gardner J. P., 2014, ArXiv e-prints
- Katz N., White S. D. M., 1993, *ApJ*, 412, 455
- Kauffmann G., 2014, ArXiv e-prints
- Kawata D., Okamoto T., Gibson B. K., Barnes D. J., Cen R., 2013, *MNRAS*, 428, 1968
- Keller B. W., Wadsley J., Benincasa S. M., Couchman H. M. P., 2014, *MNRAS*, 442, 3013
- Kim J.-h. et al., 2014, *ApJS*, 210, 14
- Kirby E. N., Bullock J. S., Boylan-Kolchin M., Kaplinghat M., Cohen J. G., 2014, *MNRAS*, 439, 1015
- Klypin A., Karachentsev I., Makarov D., Nasonova O., 2014, ArXiv e-prints
- Knollmann S. R., Knebe A., 2009, *ApJS*, 182, 608
- Kroupa P., 2001, *MNRAS*, 322, 231
- Lovell M. R. et al., 2012, *MNRAS*, 420, 2318
- Madau P., Shen S., Governato F., 2014a, *ApJL*, 789, L17
- Madau P., Weisz D. R., Conroy C., 2014b, ArXiv e-prints
- Martizzi D., Teyssier R., Moore B., 2013, *MNRAS*, 432, 1947
- Mashchenko S., Wadsley J., Couchman H. M. P., 2008, *Science*, 319, 174
- Maxwell A. J., Wadsley J., Couchman H. M. P., Mashchenko S., 2012, *ApJL*, 755, L35
- McConnachie A. W., 2012, *AJ*, 144, 4
- McQuinn K. B. W. et al., 2010, *ApJ*, 721, 297
- Menci N., Fiore F., Lamastra A., 2012, *MNRAS*, 421, 2384
- Menon H., Wesolowski L., Zheng G., Jetley P., Kale L., Quinn T., Governato F., 2014, ArXiv e-prints
- Monelli M. et al., 2010a, *ApJ*, 722, 1864
- Monelli M. et al., 2010b, *ApJ*, 720, 1225
- Moore B., Governato F., Quinn T., Stadel J., Lake G., 1998, *ApJL*, 499, L5+
- Munshi F. et al., 2013, *ApJ*, 766, 56
- Noeske K. G. et al., 2007, *ApJL*, 660, L43
- Oh S.-H., de Blok W. J. G., Brinks E., Walter F., Kennicutt, Jr. R. C., 2011, *AJ*, 141, 193
- Ott J. et al., 2012, *AJ*, 144, 123
- Pacucci F., Mesinger A., Haiman Z., 2013, ArXiv e-prints
- Pandolfi S., Evoli C., Ferrara A., Villaescusa-Navarro F., 2014, *MNRAS*, 442, 13
- Papastergis E., Martin A. M., Giovanelli R., Haynes M. P., 2011, *ApJ*, 739, 38
- Peñarrubia J., Pontzen A., Walker M. G., Kroupa S. E., 2012, *ApJL*, 759, L42
- Penzo C., Macciò A. V., Casarini L., Stinson G. S., Wadsley J., 2014, *MNRAS*, 442, 176
- Pontzen A. et al., 2010, *MNRAS*, 402, 1523
- Pontzen A., Governato F., 2012, *MNRAS*, 421, 3464
- Pontzen A., Governato F., 2014, *Nature*, 506, 171
- Pontzen A., Roskar R., Stinson G., Woods R., 2013, pynbody: N-Body/SPH analysis for python. Astrophysics Source Code Library
- Power C., Navarro J. F., Jenkins A., Frenk C. S., White S. D. M., Springel V., Stadel J., Quinn T., 2003, *MNRAS*, 338, 14
- Puech M., Hammer F., Rodrigues M., Fouquet S., Flores H., Disseau K., 2014, ArXiv e-prints
- Quinn T. R., Jetley P., Kale L. V., Gioachin F., 2013, in Parallel Science and Engineering Applications: The Charm++ Approach, Kale L. V., Abhinav B., eds., Taylor & Francis Group, CRC Press
- Read J. I., Hayfield T., Agertz O., 2010, *MNRAS*, 405, 1513
- Ritchie B. W., Thomas P. A., 2001, *MNRAS*, 323, 743
- Robertson B., Yoshida N., Springel V., Hernquist L., 2004, *ApJ*, 606, 32
- Saitoh T. R., Makino J., 2013, *ApJ*, 768, 44
- Schneider A., Anderhalden D., Macciò A. V., Diemand J., 2014, *MNRAS*, 441, L6
- Schneider A., Smith R. E., Macciò A. V., Moore B., 2012, *MNRAS*, 424, 684
- Shen S., Madau P., Conroy C., Governato F., Mayer L., 2014, *ApJ*, 792, 99
- Shen S., Wadsley J., Stinson G., 2010, *MNRAS*, 407, 1581
- Skillman E. D., Gallart C., 2002, in Astronomical Society of the Pacific Conference Series, Vol. 274, Observed HR Diagrams and Stellar Evolution, Lejeune T., Fernandes J., eds., p. 535
- Spergel D. N., Steinhardt P. J., 2000, *Physical Review Letters*, 84, 3760
- Springel V., 2005, *MNRAS*, 364, 1105
- Stinson G., Brook C., Macciò A. V., Wadsley J., Quinn T. R., Couchman H. M. P., 2012, ArXiv e-prints
- Stinson G., Seth A., Katz N., Wadsley J., Governato F., Quinn T., 2006, *MNRAS*, 373, 1074
- Stinson G. S., Brook C., Macciò A. V., Wadsley J., Quinn T. R., Couchman H. M. P., 2013, *MNRAS*, 428, 129
- Teyssier R., Pontzen A., Dubois Y., Read J. I., 2013, *MNRAS*, 429, 3068
- Tolstoy E., Hill V., Tosi M., 2009, *ARAA*, 47, 371
- Trujillo-Gomez S., Klypin A., Colin P., Ceverino D., Arraki K., Primack J., 2013, ArXiv e-prints
- Tulin S., Yu H.-B., Zurek K. M., 2013, *PRD*, 87, 115007
- van der Wel A. et al., 2011, *ApJ*, 742, 111
- Viel M., Becker G. D., Bolton J. S., Haehnelt M. G., 2013, *Phys. Rev. D*, 88, 043502
- Viel M., Lesgourgues J., Haehnelt M. G., Matarrese S., Riotto A., 2005, *PRD*, 71, 063534
- Vogelsberger M., Genel S., Sijacki D., Torrey P., Springel V., Hernquist L., 2013, *MNRAS*, 436, 3031
- Vogelsberger M., Zavala J., Simpson C., Jenkins A., 2014, ArXiv e-prints
- Wadsley J. W., Stadel J., Quinn T., 2004, *New Astronomy*, 9, 137
- Wadsley J. W., Veeravalli G., Couchman H. M. P., 2008, *MNRAS*, 387, 427
- Walker M. G., McGaugh S. S., Mateo M., Olszewski E. W., Kuzio de Naray R., 2010, *ApJL*, 717, L87
- Weisz D. R. et al., 2011, *ApJ*, 739, 5
- Weisz D. R., Dolphin A. E., Skillman E. D., Holtzman J., Gilbert K. M., Dalcanton J. J., Williams B. F., 2014, ArXiv e-prints
- Wolf J., Martinez G. D., Bullock J. S., Kaplinghat M., Geha M., Muñoz R. R., Simon J. D., Avedo F. F., 2010, *MNRAS*, 406, 1220
- Zavala J., Vogelsberger M., Walker M. G., 2013, *MNRAS*,

8 APPENDIX- FEATURES IN THE COLOR MAGNITUDE DIAGRAM

In this section we provide a few examples of how the features of artificial Color Magnitude Diagrams are able to provide useful constraints on the star formation and assembly histories of simulated galaxies when compared with observations. This discussion is aimed at the non CMD specialist.

The resolved star color-magnitude diagram (CMD) of a galaxy can be thought of as a linear combination of simple stellar populations (SSPs), i.e., populations of a single age and metallicity, such as star clusters. The goal of CMD analysis is therefore to determine the stellar mass and metallicity of each SSP that makes up the total CMD of a galaxy. Over the past 25 years, there have been over two dozen algorithms aimed at reconstructing the SFH of a galaxy based on CMD analysis, with comparisons of various techniques generally yielding consistent solutions (Skillman & Gallart 2002; Monelli et al. 2010b,a). Despite the reliability of the general methodology, there remain several outstanding challenges in accurately and precisely measuring a SFH from a CMD. In this section, we qualitatively discuss the age sensitive features available on an optical CMD, and discuss both intrinsic limitations (e.g., age-metallicity degeneracies) and other factors (e.g., CMD quality, uncertainties in stellar physics) that affect the accuracy and precision of SFH determination even in high quality data.

To help illustrate the connection between SFHs and CMDs, we make use of simulated CMDs, which allow us to clearly highlight key age-sensitive CMD features. To construct these mock CMDs, we used the SFH and age-metallicity relationship (AMR) shown in Fig. 9, as input into the CMD simulation tool from the CMD analysis software suite *MATCH* (Dolphin 2002) along with the Padova stellar evolution libraries (Girardi et al. 2010). The SFH and AMR are designed to mimic a bursty dwarf galaxy with bursts of $\text{SFR} = 10^{-3} M_{\odot}/\text{yr}$ superimposed at select times onto a constant $\text{SFR} = 10^{-4} M_{\odot}/\text{yr}$. The simulated CMDs in Fig. 10 have also been convolved with observational uncertainties (e.g., photometric errors, color and magnitude biases) that are designed to mimic an HST observation of the LMC. The CMDs are shown in the F475W (Sloan g-band) and F814W (I-band) filter combination, which is commonly used for resolved stellar population studies of nearby dwarf galaxies (Cole et al. 2007; Skillman & Gallart 2002; Dalcanton et al. 2009; Monelli et al. 2010b,a; Hidalgo et al. 2010; Weisz et al. 2014). The simulated CMDs and SFH share a common color-coding scheme, allowing for a simple translation from bursts of star formation to stars on the CMD.

Beginning at recent times, we see that stars from the youngest burst (0-0.1 Gyr; green) can be found on the main sequence (MS), as well as the blue and red core helium burning sequences (BHeBs, RHeBs) – the post-MS phase of evolution for stars more massive than a couple of solar masses. The age leverage for such young populations typically comes from both the luminosity of main sequence turnoff magnitude (MSTO; of $M_{F475W} < -3$ for an age of 0.1 Gyr) and the luminosity function of the BHeB and RHeB

stars, which are follow a nearly monotonic relationship with age (Dohm-Palmer et al. 1997). While BHeBs and RHeBs are excellent age indicators in theory, they are also rapidly evolving evolutionary phases whose physics is less certain. Uncertainties in the physical parameters (e.g., mass loss, convective overshooting) make it challenging to accurately assign absolute ages based on evolved stars alone. Instead, the MSTO provides a more secure absolute age indicator, as the models of MS stars and their evolution at the turnoff is generally better understood (Gallart et al. 2007).

The next oldest burst (0.5-0.6 Gyr; purple) has a MSTO that is less luminous than the 0-0.1 Gyr old population. Stars of this age also occupy several distinct areas on the CMD including the faint end of the BHeB and RHeB sequences, the thermally pulsating asymptotic giant branch (TP-AGB) phase, the red clump (RC; $m_{F475W} \sim 1.2$, $m_{F475W} - m_{F814W} \sim 0$). Unlike the MSTO and BHeB/RHeB, the TP-AGB and RC can be composed of stars of many difference ages and metallicities, as we discuss below. Thus, precise age determination from these features alone is difficult. Additionally, the physics of these evolved phases is still not fully understood, which further complicates our reliance on them for SFH reconstruction. Typically, the combination of the MSTO and the evolved phases (e.g., RC) yield the best constraints on the CMD, although there is still not consensus on this approach, and some prefer to only model the MSTO.

Increasingly older bursts (1-2 Gyr, orange; 5-6 Gyr, blue; 12.5-14 Gyr, red) show several common features: MSTO that decreases in luminosity with increasing look-back age, occupation of the RC, and stars that populate the red giant branch (RGB). Star-formation that occurred more than ~ 1 Gyr ago no longer has BHeB or RHeB stars, which have died. In this age range, only the youngest population (1-2 Gyr; orange) produces luminous AGB stars, while only star-formation that is at least several Gyr old produce a horizontal branch (HB). The HB is known to be sensitive to age and metallicity, with a blue HB forming for the oldest and most metal poor populations. However, uncertainties in HB models compromise its reliability as an accurate age indicator. Optimal SFH recovery comes from a CMD that extends below the oldest MSTO. For ancient SFHs, such deep CMDs contain both the oldest MSTO and the sub-giant branch (SGB), whose colors and luminosities allow for the separation of sequences as closely spaced as ~ 1 Gyr at the oldest ages possible. The loci of such ancient sequences are typically separated by 0.05-0.1 dex in color and magnitude in the F475W and F814W filters. The amount of separation between the sequence is less for filters that are not as far apart in effective wavelength (e.g., R and I), and higher signal-to-noise ratios (i.e., longer integration times) are needed to achieve the same precision on the ancient SFHs. For younger ages, such deep CMDs are guaranteed to contain the maximum amount of information possible for SFH reconstruction.

Of course, not all CMDs extend below the oldest MSTO. Due to stellar crowding effects, beyond ~ 300 kpc, the oldest MSTO of a galaxy is no longer resolvable from ground-based telescopes. Similarly, beyond ~ 1 Mpc, even HST-based CMDs are restricted to magnitudes brighter than the oldest MSTO. As a result, the majority of SFHs in the literature have been derived from CMDs that do not contain the oldest MSTO. The net effect is that the resulting

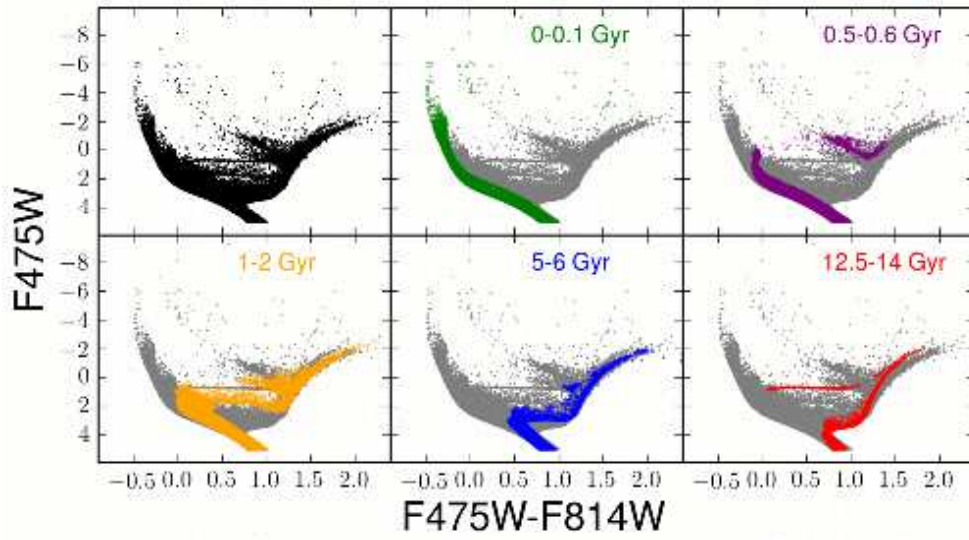


Figure 10. *Appendix A: Simulated CMDs based on the SFHs from Fig. 9, and observational uncertainties designed to mimic an HST observation of the LMC. In each panel we have highlighted the bursts of star formation from Fig. 9 in an identical color.*

SFHs are limited to age resolutions of several Gyr for ages larger than a few Gyr. The coarse age resolution of these SFHs is due to intrinsic limits of shallow CMDs. Well-known degeneracy among evolved stars (e.g., the age-metallicity degeneracy on the RGB; Cole et al. 2005) coupled with reliance on the less-certain physics of these phases of evolution that are typically overcome by the oldest MSTO, dominate the error budget for SFHs from CMDs that do not contain the oldest MSTO (Dolphin 2002; Gallart et al. 2007).

This paper has been typeset from a $\text{\TeX}/\text{\LaTeX}$ file prepared by the author.